LETTERS

Analysis of a RanGTP-regulated gradient in mitotic somatic cells

Petr Kaláb[1], Arnd Pralle[1], Ehud Y. Isacoff[1], Rebecca Heald[1] & Karsten Weis[1]

The RanGTPase cycle provides directionality to nucleocytoplasmic transport, regulating interactions between cargoes and nuclear transport receptors of the importin-β family[1,2]. The Ran–importin-β system also functions in mitotic spindle assembly and nuclear pore and nuclear envelope formation[1,3,4]. The common principle underlying these diverse functions throughout the cell cycle is thought to be anisotropy of the distribution of RanGTP (the RanGTP gradient), driven by the chromatin-associated guanine nucleotide exchange factor RCC1 (refs 1, 4, 5). However, the existence and function of a RanGTP gradient during mitosis in cells is unclear. Here we examine the Ran–importin-β system in cells by conventional and fluorescence lifetime microscopy using a biosensor, termed Rango, that increases its fluorescence resonance energy transfer signal when released from importin-β by RanGTP. Rango is predominantly free in mitotic cells, but is further liberated around mitotic chromatin. *In vitro* experiments and modelling show that this localized increase of free cargoes corresponds to changes in RanGTP concentration sufficient to stabilize microtubules in extracts. In cells, the Ran–importin-β–cargo gradient kinetically promotes spindle formation but is largely dispensable once the spindle has been established. Consistent with previous reports[6–8], we observe that the Ran system also affects spindle pole formation and chromosome congression *in vivo*. Our results demonstrate that conserved Ran-regulated pathways are involved in multiple, parallel processes required for spindle function, but that their relative contribution differs in chromatin- versus centrosome/kinetochore-driven spindle assembly systems.

To visualize the spatial distribution of the Ran system in living cells, we developed a fluorescence resonance energy transfer (FRET) biosensor termed Rango (Ran-regulated importin-β cargo) that increases its FRET signal when liberated from importin-β by RanGTP (Fig. 1a). Rango contains the importin-β-binding domain (IBB) of human snurportin 1 (ref. 9) flanked by yellow fluorescent protein (EYFP) at the amino terminus and cerulean CFP[10] at the carboxy terminus. In contrast to a sensor based on the IBB of importin-α1 (ref. 11), Rango displayed little toxicity in somatic cells and did not affect cell cycle progression (data not shown). Upon excitation at 435 nm, Rango exhibited higher emission intensity at the YFP acceptor peak (I_{FRET} at 525 nm) than at the CFP donor wavelength (I_{CFP} at 474 nm), indicative of FRET (Fig. 1b). The ratio of I_{FRET} to I_{CFP} decreased significantly in the presence of importin-β, and this effect was completely reversed by RanGTP, which induced the dissociation of Rango from importin-β (Fig. 1b). In extracts prepared from human HeLa cells, the Rango probe also dynamically reported on the levels of importin-β binding and RanGTP-mediated cargo release (Supplementary Fig. S1).

To quantify the importin-β–cargo interaction using Rango, we measured I_{FRET}/I_{CFP} ratio changes in a spectrofluorimeter upon addition of increasing concentrations of importin-β, and plotted the calculated fractional occupancy of the sensor based on Rango's experimentally determined apparent dissociation constant for importin-β of 2 nM (Fig. 1c; see also Supplementary Fig. S2). At the same time, we measured changes in the fluorescence lifetime of the Rango cerulean donor using fluorescence lifetime imaging microscopy (FLIM; Fig. 1c). As the decrease of the quantum yield due to FRET is accurately reported by a decrease of the donor lifetime (τ_{donor}), FLIM offers a concentration- and cross-bleed-independent FRET detection method that can be used to quantify molecule interactions *in vitro* and in living cells[12,13]. As expected, the Rango FRET signal decreased with an increase in its fractional occupancy by importin-β, and the average τ_{donor} increased from 2.35 ns to 2.85 ns at 23 °C, and from 2.08 ns to 2.60 ns at 30 °C (Fig. 1c).

Rango introduced into cells by either transient expression or microinjection was efficiently imported into nuclei, where the average τ_{donor} was 2.21 ± 0.07 ns (mean ± s.d., $N = 10$), indicating that nuclear Rango was almost exclusively free (Fig. 1d). Introduction of the Ran-insensitive importin-$\beta_{71–876}$ caused the Rango probe to localize to both the cytoplasm and the nucleus, and the average τ_{donor} throughout the cell increased to 2.51 ± 0.05 ns ($N = 7$), similar to the lifetime of a FRET-deficient cerulean control protein (2.59 ± 0.05 ns, $N = 15$), indicating that the increase in Rango sensor lifetime reflected a loss of FRET due to importin-β binding (Fig. 1d; see also Supplementary Fig. S3). We also performed acceptor bleach experiments using confocal laser scanning microscopy that showed that Rango is mostly free in the nucleus (Supplementary Fig. S4), confirming our FLIM analysis. The strong nuclear accumulation of Rango prevented us from analysing its behaviour in the interphase cytoplasm under normal conditions. However, microinjection of low concentrations of wheat germ agglutinin (WGA) partially blocked nuclear transport, causing some Rango to be retained in the cytoplasm, where it displayed lower FRET levels indicative of importin-β binding (Fig. 1e). Thus, Rango enables the RanGTP-dependent disassembly of importin-β–cargo complexes in the nucleus of interphase cells to be visualized.

To measure quantitative differences in Rango binding to importin-β during mitosis, FLIM data were recorded in mitotic HeLa cells transfected with Rango, and Rango's fractional occupancy was estimated based on our *in vitro* calibration data (Fig. 1c). Rango localized throughout the cytoplasm and was largely excluded from mitotic chromosomes (Fig. 2a). In all mitotic HeLa cells in which a gradient could be recorded (36 out of 46 cells; Supplementary Fig. S5), we detected a region of significantly higher FRET (shorter τ_{donor}) surrounding the chromatin ($\tau_{donor} = 2.21 \pm 0.06$ ns ($N = 36$), corresponding to a Rango–importin-β occupancy of 18 ± 9%) and the FRET signal gradually decreased towards the cell periphery ($\tau_{donor} = 2.29 \pm 0.07$ ns, 31 ± 12% occupancy; Fig. 2). Although the FRET values varied considerably between cells (see Supplementary Fig. S5), the average difference of τ_{donor} between

[1]Department of Molecular and Cell Biology, University of California, Berkeley, California 94720-3200, USA.

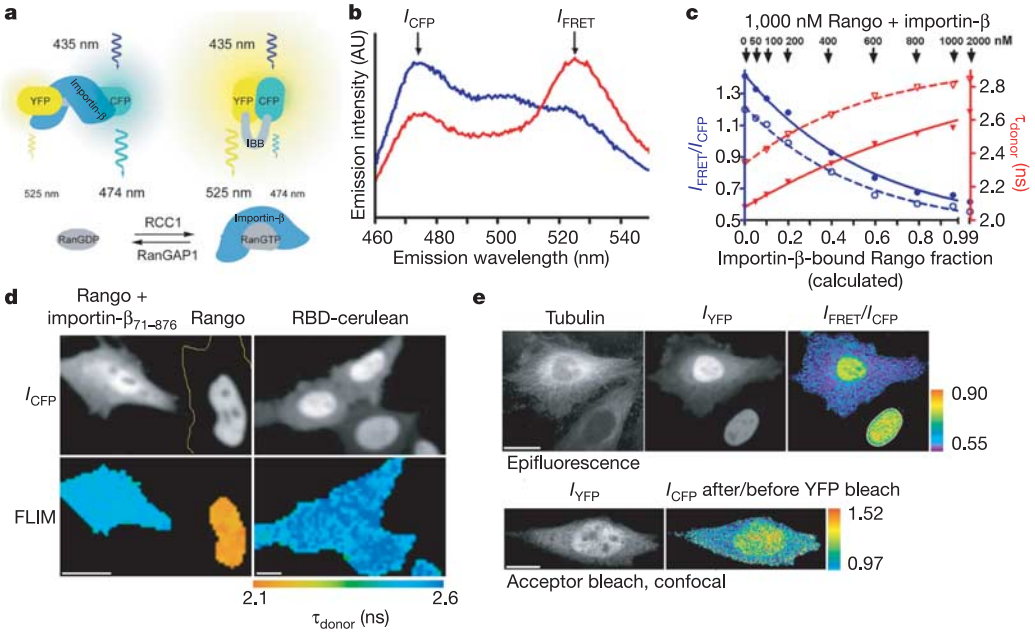

Figure 1 | Characterization of the Rango–importin-β interaction *in vitro*. **a**, Schematic of Rango probe. **b**, Emission spectrum of 0.5 μM Rango excited at 435 nm in the presence of 0.2 μM RCC1, 1 μM importin-β, 2 μM Ran and either 1 mM GDP (blue line) or 1 mM GTP (red line). Arrows indicate I_{CFP} (474 nm) and I_{FRET} (525 nm) emission. AU, arbitrary units. **c**, Rango FRET efficiency determined as I_{FRET}/I_{CFP} ratio (blue), or cerulean fluorescence lifetime (red), upon titration of 1,000 nM Rango with 0–2,000 nM importin-β *in vitro* at 23 °C (dashed lines) and at 30 °C (solid lines). The fractional occupancy of Rango bound to importin-β was calculated. **d**, Donor CFP intensity (top) and pseudo-coloured cerulean fluorescence lifetime (bottom) of interphase cells expressing Rango (left panels) or an RBD-cerulean control (right panels). A Rango-expressing cell on the right is outlined; the cell on the left was injected with importin-β_{71-876}. **e**, Fluorescence images of cells co-injected with Rango, importin-β, 0.5 mg ml^{-1} WGA and rhodamine-labelled tubulin. Scale bars, 20 μm.

chromatin and mitotic cytoplasm was 0.08 ± 0.03 ns, corresponding to a 13 ± 5% decrease in Rango–importin-β binding around chromatin.

These results were also qualitatively confirmed by acceptor photobleaching experiments (Supplementary Figs S6 and S7). The observed gradient did not result from concentration-induced errors in our FLIM measurements, as a modified version of Rango (k-Rango)—which was fused to the DNA-binding domain of the human centromere protein CENP-B[14]—displayed a similar FLIM profile despite a very different localization pattern (Fig. 2a, b). Furthermore, variations in the cargo dissociation constant (in a range between 0.5 and 50 nM) are expected to have only very minor effects on the importin-β occupancy in the mitotic cytoplasm (Supplementary Fig. S8 and data not shown). Thus, our FRET analyses indicate that at equilibrium, high RanGTP concentrations and/or limited importin-β cargo-binding sites exist in the mitotic cytoplasm. Furthermore, they demonstrate the presence of a significant RanGTP-regulated free cargo gradient extending from mitotic chromatin.

To compare embryonic and somatic systems under identical detection conditions, we acquired epifluorescence ratio images in metaphase *Xenopus* egg extracts containing Rango and in HeLa cells microinjected with Rango. Rhodamine-tubulin was used to label microtubules in both cases (Fig. 3a). The dimensions of the cargo gradient were analysed by linescan analysis (Fig. 3b, Methods). Elevated levels of free Rango were observed in *Xenopus* extract spindles in an area extending 15–20 μm from the chromatin (Fig. 4a), as seen previously with an importin-α1-based importin-β sensor (YIC)[11]. Although the gradient in the *Xenopus* extract dropped over a greater distance, and was thus significantly less steep than in HeLa cells (3–4 μm), in both systems it reached to the spindle poles (indicated by asterisks in Fig. 3a, b).

The existence of significant concentrations of free importin-β cargoes throughout the mitotic cytoplasm is inconsistent with simple

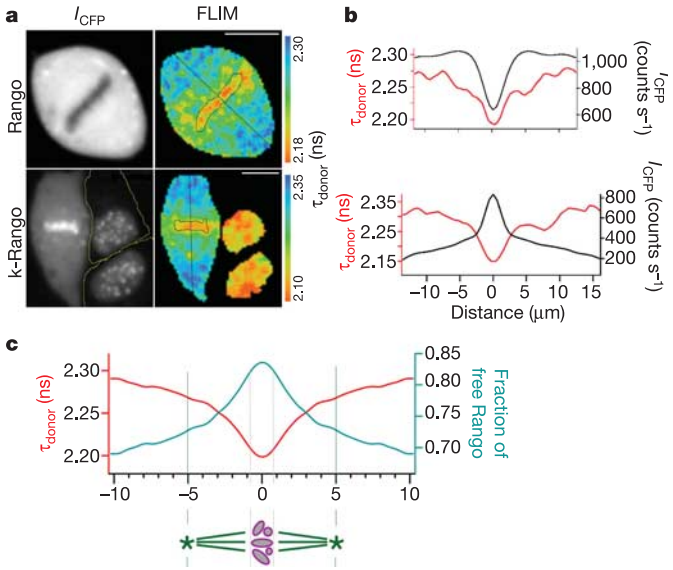

Figure 2 | Detection of the Ran-regulated mitotic Rango gradient in HeLa cells by FLIM. **a**, Donor fluorescence (left) and pseudo-coloured FLIM image (right) of a mitotic HeLa cell expressing Rango (top panels) or k-Rango (bottom panels). Chromatin and linescan positions are outlined in the FLIM image. Scale bar, 10 μm **b**, Linescan of donor fluorescence lifetime, averaged over 5 μm (red), and donor intensity (black) obtained from **a**. **c**, Average linescans of Rango donor fluorescence lifetime (eight gradients from four HeLa cells, exploiting axial symmetry in the system) (red) and corresponding linescan of unbound Rango fraction (cyan) calculated using the titration curve in Fig. 1c. The average positions of chromatin, mitotic spindle and centrosomes are indicated.

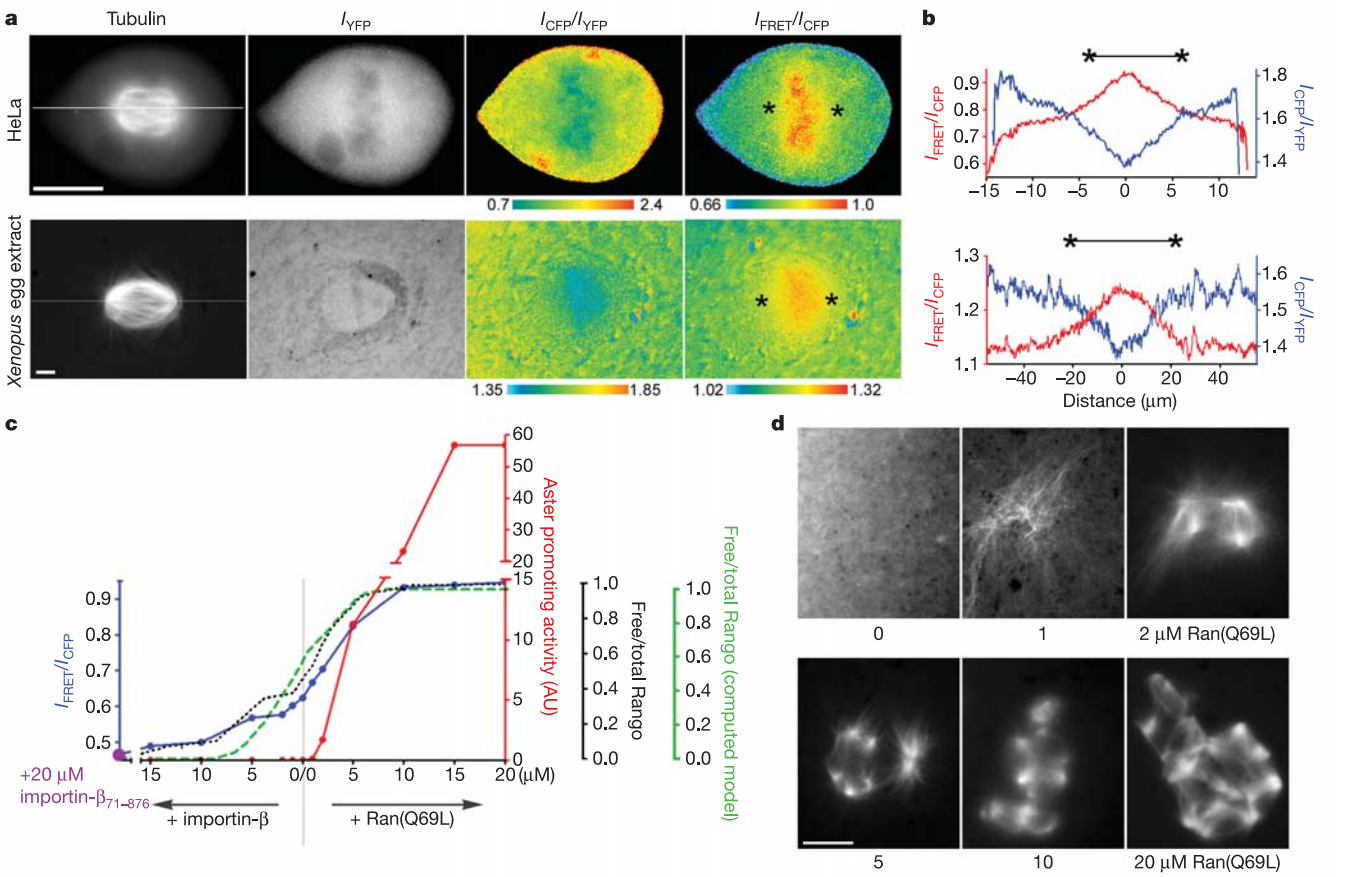

Figure 3 | Comparison of Rango gradient in mitotic HeLa cells and meiotic *X. laevis* egg extracts. a, Rango FRET signal in a metaphase HeLa cell microinjected with 18 μM Rango and 1.6 μM rhodamine-tubulin (top), and in *X. laevis* metaphase extract supplemented with 2 μM Rango and 0.5 μM rhodamine-tubulin (bottom). The asterisks indicate the position of spindle poles. The Rango signal in *Xenopus* extract was not background-subtracted, causing an overall shift of the ratio values compared to the HeLa cell. **b**, I_{FRET}/I_{CFP} and I_{CFP}/I_{YFP} ratio linescans (3 μm in HeLa, 5 μm in egg extract) corresponding to the white line in rhodamine-tubulin panels of **a**. **c**, 1 μM Rango and 0.5 μM rhodamine-tubulin was added to mitotic *X. laevis* egg extract, aliquots were supplemented with increasing concentrations of Ran(Q69L) or importin-β and the I_{FRET}/I_{CFP} ratio was determined by spectrofluorimetry (blue). The fraction of importin-β-free Rango (black) was calculated using *in vitro* titration data (Fig. 1d, see Methods). The response of a minimal computational system (green) was calculated as described in Supplementary Fig. S8. Aster promoting activity (red) was assayed as the average number of mitotic microtubule asters per visual field in fixed samples (AU, see Methods). Note that the scale of aster promoting activity is compressed for values above 20 AU. **d**, Images of rhodamine-tubulin-labelled microtubule structures taken in non-fixed extract samples at the end of analysis. Scale bars, 10 μm.

models that propose complete binding and inhibition of importin-β-regulated activities in the mitotic cytoplasm[1]. However, it agrees qualitatively with computer simulations of a minimal Ran system that have been used to calculate free RanGTP concentrations[15,16] and with our attempts to model importin-β–cargo interactions in cells or extracts (Fig. 3c; see also Supplementary Fig. S8). To investigate whether the observed increase in Ran-regulated cargo liberation around chromatin might regulate microtubule dynamics in mitosis, we performed titration experiments with RanGTP and importin-β in *Xenopus* egg extracts, monitoring, in parallel, the interaction of Rango with importin-β and changes in microtubule morphology (Fig. 3c, d). In the absence of exogenous Ran and importin-β, only 52 ± 5% ($N = 5$) of Rango was bound to importin-β, and yet the high fraction of free cargoes in the extract did not promote microtubule polymerization (Fig. 3d). However, when the RanGTP concentration was increased by the addition of 1 μM Ran(Q69L), decreasing Rango occupancy by 8 ± 5% ($N = 5$), bundled microtubules formed. A further increase in RanGTP (2–5 μM Ran(Q69L)) induced formation of relatively large microtubule asters, whereas even higher concentrations (10–30 μM Ran(Q69L)) induced formation of structures with shorter radiating microtubules and more focused centres (Fig. 3d). These results show that the cargo liberation observed around mitotic HeLa chromosomes is quantitatively similar to the increase in free cargoes sufficient to stimulate microtubule polymerization in extracts. Furthermore, these data suggest that the Ran–importin-β system is poised to respond to small increases in RanGTP concentration from the physiological set point found in the mitotic cytoplasm to regulate microtubule dynamics and organization.

Whereas the Rango FRET signal plateaued at 10 μM of added Ran(Q69L), the number of microtubule asters more than doubled with further increases of Ran(Q69L) to 15–30 μM. This result implies the existence of a class of activity for which regulation in the extracts requires a much higher RanGTP concentration than does a Rango-like cargo. Alternatively, reactions induced by high RanGTP concentrations in the cytoplasmic extracts may mimic conditions of limited diffusion (for example, at the chromatin–cytoplasm interface).

To assess directly the functional significance of the Ran–importin-β system during mitosis in somatic cells, we microinjected a panel of dominant-negative proteins to inhibit the Rango gradient in HeLa cells in either prophase or metaphase. Microinjection of Ran(Q69L) induced the formation of ectopic microtubule asters in the cytoplasm of some cells (Fig. 4b, arrows; see also Supplementary Fig. S9a and Supplementary Table 1) similar to the asters observed in *Xenopus* extracts (Fig. 3d). However, spindles remained intact when metaphase cells were injected with importin-$\beta_{71–876}$, a potent dominant-negative

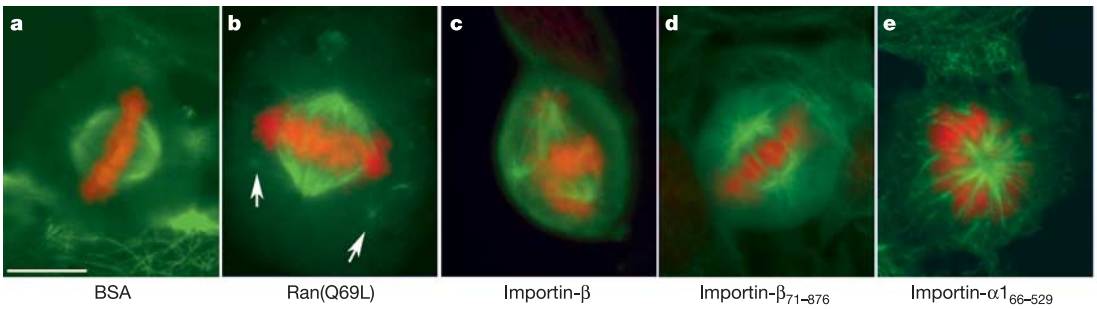

Figure 4 | Mitotic spindle phenotypes induced by Ran system perturbations in somatic cells. a–e, Mitotic phenotypes induced by microinjection of BSA (**a**; nonspecific control, 550 μM in the microinjection needle), Ran(Q69L) (**b**; 420 μM), importin-β (**c**; 80 μM), importin-$\beta_{71–876}$ (**d**; 420 μM) and importin-$\alpha 1_{66–529}$ (**e**; 310 μM). DNA is coloured red (Hoechst 33342 staining); α-tubulin fluorescence is shown in green. Scale bar, 10 μm.

inhibitor of chromatin-induced microtubule dynamics and spindle assembly in *Xenopus* extracts[11,17]. Instead, the most prominent phenotype induced by injection of either importin-$\beta_{71–876}$ or importin-$\alpha 1_{66–529}$ in early mitosis was a delay at the prometaphase to metaphase transition, frequently associated with monoastral microtubule arrays (Fig. 4d, e; see also Supplementary Fig. S9 and Supplementary Table 1). The induction of large monoastral microtubule structures indicates that the normal progression from a radial to bipolar microtubule arrangement during prophase requires an intact cargo gradient in cells. This conclusion is consistent with modelling studies[18] and suggests that Ran-gradient-regulated stabilization of microtubules around chromatin supports a search and capture mechanism of microtubule–kinetochore attachment. Notably, in addition to a delay in prometaphase, injection of full-length importin-β also induced split spindle poles (Fig. 4c; see also Supplementary Table 1), consistent with a model that Ran and importin-β may function in the regulation of centrosomes[6].

Our results suggest that the RanGTP gradient provides a significant kinetic advantage during the early stages of spindle assembly in primarily centrosome-driven somatic cells. However, in contrast to the situation for extracts, once a bipolar spindle is established in cells, the RanGTP gradient and the Ran–importin-β cargo regulation appears to be largely dispensable for spindle integrity. This indicates that in cells, mitotic spindles are built and maintained by multiple, parallel pathways, and demonstrates that centrosome/kinetochore- and chromatin-driven systems differentially use Ran and importin-β to promote mitotic spindle assembly. Notably, in both HeLa cells and *Xenopus* egg extracts, the steepness of the Ran-regulated gradient seems to be adjusted to the enormous differences in the spindle size (Fig. 3a, b). This organization permits relative differences in cargo occupancy to influence events between the spindle poles and chromatin in both systems.

On the basis of our results, we propose that the mitotic cytoplasm operates near a physiological threshold in which positive and negative regulators are at equilibrium. Such a system would be poised to break the threshold in response to small local changes in RanGTP concentration and, for example, influence microtubule stability around chromatin in prophase cells. This behaviour may allow the Ran–importin-β pathway to locally regulate its targets and to signal both chromatin- and centrosome-driven events in mitosis.

METHODS

Cloning and protein expression. A description of all the clones used in this study and details of protein expression are given in the Supplementary Methods.

Fractional occupancy of Rango titrated with importin-β. Rango–importin-β fractional occupancy (Fig. 1c) was calculated as follows:

$$K_d = \beta C / C_{\beta C}$$

$$K_d = (\beta_T - C_{\beta C})(C_T - C_{\beta C})/C_{\beta C}$$

where $C_{\beta C}$ is the concentration of the importin-β–cargo complex (fractional occupancy), β is the concentration of free importin-β, β_T is the total concentration of importin-β, C is the concentration of free importin-β cargo, C_T is the total concentration of importin-β cargo and K_d is the dissociation constant, resulting in $C_{\beta C} = 0.5(C_T + \beta_T + K_d - \sqrt{(C_T + \beta_T + K_d)^2 - 4\beta_T C_T})$.

Spectrophotometry. Emission spectra were analysed with a Fluorolog 2 spectrofluorimeter controlled by Datamax 2.2 (Jobin Yvon Spex) and the Grams 3.04 II software package (Galactic Industries). Details are given in the Supplementary Methods.

Cell culture and transfection. BHK21 cells and HeLa cells were purchased from ATCC. tsBN2 cells were a gift of T. Nishimoto and M. Dasso. Cells were maintained in Opti-MEM (Gibco, Invitrogen) with 4% fetal bovine serum at 37 °C, 5% CO_2, except for tsBN2 cells, which were kept at 33 °C, 5% CO_2. For cell transfection, Fugene 6 (Roche Diagnostics) was used according to the manufacturer's protocol.

Microinjection and immunofluorescence. Cells were microinjected using an Olympus IX71 microscope equipped with a FemtoJet microinjector (Eppendorf), and analysed by immunofluorescence to visualize microtubules and DNA using an Olympus BX51 microscope equipped with a Hamamatsu CA 742-98 CCD camera. Details are given in the Supplementary Methods.

Live cell epifluorescence imaging. Live cell epifluorescence ratio imaging was performed with a Nikon E600 microscope equipped with a Hamamatsu C4742-98 CCD camera as described previously[11]. Additional details are given in the Supplementary Methods.

Fluorescence lifetime and confocal microscopy. Data sets of spatially resolved, time-correlated single photon counting (TCSPC) were acquired on an inverted Zeiss LSM510 Axiovert 200M microscope equipped with a TCSPC controller (Becker & Hickl SPC-730). Confocal microscopy was performed with a Zeiss LSM 510 META laser scanning confocal microscope. Additional details are provided in the Supplementary Methods.

***Xenopus laevis* egg extracts.** Assays for the detection of the Rango I_{FRET}/I_{CFP} signal during mitotic spindle assembly in *X. laevis* egg extracts were performed as described previously[11] with rhodamine-tubulin and 2 μM Rango in the extract instead of YIC. Details are given in the Supplementary Methods.

Statistical analyses. Statistical analyses were performed with Excel (Microsoft) and with GraphPad Prism version 4.00 for Windows, GraphPad Software (http://www.graphpad.com).

Received 18 November 2005; accepted 18 January 2006.

1. Weis, K. Regulating access to the genome: nucleocytoplasmic transport throughout the cell cycle. *Cell* **112**, 441–451 (2003).
2. Pemberton, L. F. & Paschal, B. M. Mechanisms of receptor-mediated nuclear import and nuclear export. *Traffic* **6**, 187–198 (2005).
3. Hetzer, M., Gruss, O. J. & Mattaj, I. W. The Ran GTPase as a marker of chromosome position in spindle formation and nuclear envelope assembly. *Nature Cell Biol.* **4**, E177–E184 (2002).
4. Harel, A. & Forbes, D. J. Importin-β: conducting a much larger cellular symphony. *Mol. Cell* **16**, 319–330 (2004).
5. Hetzer, M., Bilbao-Cortes, D., Walther, T. C., Gruss, O. J. & Mattaj, I. W. GTP hydrolysis by Ran is required for nuclear envelope assembly. *Mol. Cell* **5**, 1013–1024 (2000).
6. Ciciarello, M. *et al.* Importin-β is transported to spindle poles during mitosis and regulates Ran-dependent spindle assembly factors in mammalian cells. *J. Cell Sci.* **117**, 6511–6522 (2004).
7. Arnaoutov, A. & Dasso, M. The Ran GTPase regulates kinetochore function. *Dev. Cell* **5**, 99–111 (2003).

8. Arnaoutov, A. *et al.* Crm1 is a mitotic effector of Ran-GTP in somatic cells. *Nature Cell Biol.* **7,** 626–632 (2005).
9. Huber, J., Dickmanns, A. & Luhrmann, R. The importin-β binding domain of snurportin1 is responsible for the Ran- and energy-independent nuclear import of spliceosomal U snRNPs *in vitro*. *J. Cell Biol.* **156,** 467–479 (2002).
10. Rizzo, M. A., Springer, G. H., Granada, B. & Piston, D. W. An improved cyan fluorescent protein variant useful for FRET. *Nature Biotechnol.* **22,** 445–449 (2004).
11. Kalab, P., Weis, K. & Heald, R. Visualization of a Ran-GTP gradient in interphase and mitotic *Xenopus* egg extracts. *Science* **295,** 2452–2456 (2002).
12. Suhling, K., French, P. M. & Phillips, D. Time-resolved fluorescence microscopy. *Photochem. Photobiol. Sci.* **4,** 13–22 (2005).
13. Becker, W. *et al.* Fluorescence lifetime imaging by time-correlated single-photon counting. *Microsc. Res. Tech.* **63,** 58–66 (2004).
14. Shelby, R. D., Hahn, K. M. & Sullivan, K. F. Dynamic elastic behaviour of alpha-satellite DNA domains visualized *in situ in* living human cells. *J. Cell Biol.* **135,** 545–557 (1996).
15. Gorlich, D., Seewald, M. J. & Ribbeck, K. Characterization of Ran-driven cargo transport and the RanGTPase system by kinetic measurements and computer simulation. *EMBO J.* **22,** 1088–1100 (2003).
16. Riddick, G. & Macara, I. G. A systems analysis of importin-α-β mediated nuclear protein import. *J. Cell Biol.* **168,** 1027–1038 (2005).
17. Nachury, M. V. *et al.* Importin-β is a mitotic target of the small GTPase Ran in spindle assembly. *Cell* **104,** 95–106 (2001).
18. Wollman, R. *et al.* Efficient chromosome capture requires a bias in the 'search-and-capture' process during mitotic-spindle assembly. *Curr. Biol.* **15,** 828–832 (2005).

Supplementary Information is linked to the online version of the paper at www.nature.com/nature.

Acknowledgements The authors wish to thank T. Nishimoto, M. Dasso, J. Fang, M. A. Rizzo, D. W. Piston and F. Melchior for providing reagents, and C. Weirich for performing fluorescence polarization assays. We are grateful to A. Arnaoutov for discussion and sharing unpublished results, C. Weirich, M. Blower, A. Madrid and H. Aaron for critical reading of the manuscript, and members of the Heald and Weis laboratories for discussions. The research described in this article was supported in part by Philip Morris USA Inc. and Philip Morris International (R.H.), and by grants from the National Institute of Health (E.Y.I., R.H. and K.W.).

Author Contributions P.K. and A.P. contributed equally to this project.

Author Information Reprints and permissions information is available at npg.nature.com/reprintsandpermissions. The authors declare no competing financial interests. Correspondence and requests for materials should be addressed to R.H. (heald@socrates.berkeley.edu) or K.W. (kweis@berkeley.edu).